

## Decoupling functional mechanisms of adaptive encoding

NICHOLAS A. LESICA & GARRETT B. STANLEY

*Division of Engineering & Applied Sciences, 321 Pierce Hall, 29 Oxford Street, Harvard University, Cambridge, MA 02138, USA*

*(Received 10 March 2005; revised 23 June 2005; accepted 4 August 2005)*

### Abstract

In a natural setting, adaptive mechanisms constantly modulate the encoding properties of sensory neurons in response to changes in the external environment. Recent experiments have revealed that adaptation affects both the spatiotemporal integration properties and baseline membrane potential of sensory neurons. However, the precise functional role of adaptation remains an open question, due in part to contradictory experimental results. Here, we develop a framework to characterize adaptive encoding, including a cascade model with a time-varying receptive field (reflecting spatiotemporal integration properties) and offset (reflecting baseline membrane potential), and a recursive technique for tracking changes in the model parameters during a single stimulus/response trial. Simulated and experimental responses from retinal neurons are used to track adaptive changes in receptive field structure and offset during nonstationary stimulation. Due to the nonlinear nature of spiking neurons, the parameters of the receptive field and offset must be estimated simultaneously, or changes in the offset (or even in the statistical distribution of the stimulus) can mask, confound, or create the illusion of adaptive changes in the receptive field. Our analysis suggests that these confounding effects may be at the root of the inconsistency in the literature and shows that seemingly conflicting experimental results can be reconciled within our framework.

**Keywords:** *Retina, adaptation, vision, model, estimation*

### Introduction

Many sensory neurons adapt their response properties to changes in the visual environment. In the early visual pathway, studies of adaptation have shown dramatic changes in encoding properties in response to changes in the mean and contrast of the visual stimulus (Shapley & Victor 1978; Movshon & Lennie 1979; Shapley & Enroth-Cugell 1984). Adaptive function is particularly critical in a natural setting, where the statistical distribution of sensory stimuli is constantly changing. For example, the mean or contrast of the stimulus within the receptive field of a visual neuron can change drastically as a result of changes in illumination, object and/or observer motion, or saccades across the visual scene. In the face of such changes, it has been proposed that adaptive mechanisms enable sensory neurons to maximize their differential sensitivity to the current stimulus (Shapley & Enroth-Cugell 1984) and optimize the transmission of information to downstream neurons (Brenner et al. 2000; Fairhall et al. 2001). However, despite the ubiquitous nature of adaptation and the profound manner in

---

Correspondence: N. A. Lesica, Division of Engineering & Applied Sciences, 321 Pierce Hall, 29 Oxford Street, Harvard University, Cambridge, MA 02138, USA. Tel: (617) 495-3206. Fax: (617) 496-0601. E-mail: lesica@fas.harvard.edu

which it affects the response properties of sensory neurons, its precise functional role remains an open question.

In the early visual pathway, adaptation has been shown to occur on multiple time scales, as encoding properties are adjusted in response to changes in the statistics of the stimulus (Shapley & Victor 1978; Movshon & Lennie 1979; Shapley & Enroth-Cugell 1984; Smirnakis et al. 1997). Adaptation has been shown to produce changes in both the spatiotemporal integration properties and baseline membrane potential of a neuron (Carandini & Ferster 1997; Sanchez-Vives et al. 2000; Baccus & Meister 2002; Solomon et al. 2004) and a recent study has shown that these changes are due to both synaptic and intrinsic mechanisms (Zaghloul et al. 2005). The spatiotemporal integration properties of a neuron determine the relationship between the visual stimulus and modulations in membrane potential, reflecting the relative strength of synaptic inputs from upstream neurons. The baseline membrane potential sets the operating point of the neuron with respect to its spike generation threshold and determines the fraction of the modulations in membrane potential that are visible in the firing rate response. For example, the same stimulus-driven modulations in membrane potential can result in a high firing rate if the membrane is depolarized (and the potential is already close the spike threshold), or no spikes at all if the membrane is hyperpolarized. Thus, adaptive changes in the spatiotemporal integration properties and baseline membrane potential act together to determine the response properties of the neuron.

Studies of the dynamics of adaptive encoding have produced conflicting results. For example, studies of contrast adaptation in the rabbit retina are inconsistent in their descriptions of the persistence of the decrease in gain that follows an increase in contrast. Some studies suggest that following an increase in contrast, the gain will decrease rapidly (in less than one second) and then remain constant while the contrast remains high (Baccus & Meister 2002), while others suggest that the gain will decline slowly over a period of seconds (Smirnakis et al. 1997; Brown & Masland 2001). To investigate this inconsistency and provide an accurate characterization of adaptive function, a framework must be developed in which each form of adaptation can be uniquely characterized.

The functional role of adaptation is best investigated within the context of an encoding model that captures the transformation from visual stimulus to neural firing activity. Here, we develop a cascade model of visual encoding based on observations of adaptive function in the visual pathway, with adaptive components reflecting spatiotemporal integration properties and baseline membrane potential. We also develop a recursive estimation approach that allows each component of the cascade to be identified uniquely from extracellular observations of the neural response, and avoids the potentially confounding effects of the nonlinear encoding properties of the neuron on the estimation of model parameters. Simulated and experimental responses from neurons in the retina are used to demonstrate that the function of simultaneously active mechanisms can be decoupled under adaptive conditions during a single stimulus/response trial. Our analysis provides insight into how changes in spatiotemporal integration properties and baseline membrane potential interact to modulate encoding properties during nonstationary stimulation, and also suggests a potential reconciliation of the conflicting experimental results described above.

### **Adaptive encoding in the early visual pathway**

A simple illustration of adaptive encoding can be observed during a contrast switching experiment in the retina, in which the visual stimulus alternates between low and high contrast. The mean firing rate of a retinal ganglion cell over 15 repeats of a contrast switching full-field white-noise stimulus is shown in Figure 1.

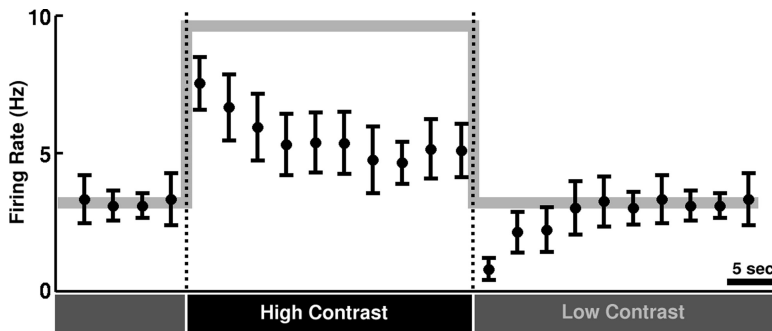


Figure 1. Adaptive encoding in the early visual pathway. The responses of a retinal ganglion cell to a spatially uniform Gaussian white-noise stimulus were recorded extracellularly. Each 60 second trial contained 30 seconds of stimulus at 35% contrast followed by 30 seconds of stimulus at 5% contrast, and a new realization of the white-noise was generated for each trial. The mean firing rate of the neuron over 15 trials is shown in 3 second intervals (black, error bars represent one standard deviation). The mean firing rate that would be expected for a non-adaptive system (based on a linear increase from the mean firing rate before the switch from low to high contrast) is shown in gray. The contrast of the stimulus is indicated below the horizontal axis.

These experiments were performed in the laboratory of Markus Meister at Harvard University and details of the preparation are given in Baccus and Meister (2002). After the switch from low to high contrast, the firing rate of the neuron increases rapidly, then decreases gradually, until reaching steady state after approximately 10 seconds. Conversely, after the switch from high to low contrast, the firing rate of the neuron rapidly decreases, then gradually increases, finally reaching a new steady state. While the switch from low to high contrast would result in an increase in firing rate in the absence of adaptation (as shown in gray, based on a linear increase from the mean firing rate before the switch), the initial sub-linear increase and the gradual decay in firing rate following the switch are a result of the function of adaptive mechanisms and cannot be explained by a time-invariant model of encoding.

#### *A model of adaptive encoding*

The response dynamics shown in Figure 1 are the result of the function of several adaptive mechanisms that produce changes in gain, frequency tuning properties, and baseline membrane potential on multiple time scales (Baccus & Meister 2002). In order to understand the role of these adaptive changes in visual encoding, it is helpful to consider adaptive function in the context of an encoding model. If the design of the model accurately reflects the nature of the system under investigation, then changes in the parameters that describe the different components of the model can be related to the function of underlying neural mechanisms.

The firing activity of many types of visual neurons can be characterized by a linear-nonlinear (LN) cascade model consisting of a linear spatiotemporal receptive field (RF) and a rectifying static nonlinearity (Hunter & Korenberg 1986; Reid et al. 1997; Chichilnisky 2001; Baccus & Meister 2002). Here, we develop a particular form of the LN cascade model, shown in Figure 2, based on observations of adaptive function in the early visual pathway as described above.

The encoding model developed here includes an adaptive RF (to capture changes in gain and frequency tuning properties that are associated with the spatiotemporal integration properties of the neuron) and an adaptive offset (to reflect changes in baseline membrane potential), along with a fixed static nonlinear rectification function. The parameters of the

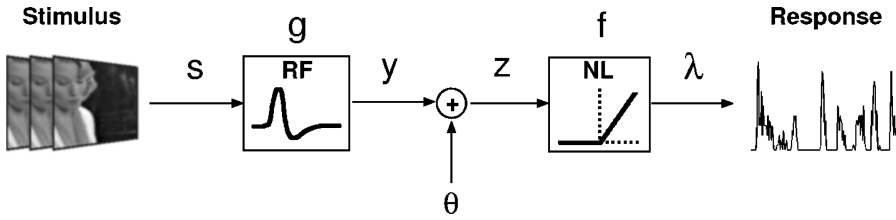


Figure 2. An LN cascade model of visual encoding. The spatiotemporal visual stimulus  $s$  is convolved with a time-varying spatiotemporal RF  $g$  to yield the intermediate signal  $y$ . This signal is then combined with time-varying offset  $\theta$  to yield the generating function  $z$ . The generating function is passed through a static nonlinearity  $f$  to produce the firing rate  $\lambda$ .

encoding model are intended to correspond to properties of the underlying neural system. However, because the model is functional in nature and designed to characterize firing rate responses to visual stimuli rather than modulations in membrane potential (and its parameters are estimated from extracellular rather than intracellular observations of the response), the correspondence between model parameters and intracellular quantities is indirect.

In the first stage of the LN cascade encoding model shown in Figure 2, the visual stimulus  $s$  is passed through the time-varying linear spatiotemporal RF  $g$  to yield the filtered stimulus  $y$ , which reflects the stimulus-driven modulations in the membrane potential of the neuron. The offset  $\theta$  is added to the filtered stimulus  $y$  before the static nonlinearity to shift the operating point of the model with respect to the rectification threshold. It is important to note that the offset captures only those changes in the membrane potential that are not accounted for by the filtering of the visual stimulus in the RF. For example, although a decrease in the mean of the stimulus could result in a direct decrease in the mean of the membrane potential, this change would be reflected in the filtered stimulus  $y$ , not in the offset. However, if this decrease in the mean of the stimulus also causes a change in the baseline membrane potential via some indirect adaptive mechanism, that change would be reflected in the offset  $\theta$ .

The filtered and offset stimulus  $z$ , known as the *generating function*, is passed through a rectifying static nonlinearity  $f(\cdot)$  to yield the non-negative firing rate  $\lambda$ . By fixing the static nonlinearity, adaptive changes in the encoding model are forced into changes in the RF  $g$  or offset  $\theta$ . This avoids ambiguity, as, for instance, changes in gain could be mapped either to the RF or to the slope of the static nonlinearity. The LN cascade encoding model is described in more detail in the Appendix.

### *Estimation of model parameters*

Because multiple adaptive mechanisms may be simultaneously active during visual encoding, it is imperative that the approach employed for analysis is able to uniquely identify changes in each component of the model. If the model structure underlying the parameter estimation process is misspecified (for example, if standard reverse correlation is used and the static nonlinearity and/or offset of the encoding model in Figure 2 are neglected), changes in the baseline membrane potential, or even in the statistical properties of the stimulus can be reflected as changes in spatiotemporal integration properties.

Consider the reduced encoding model defined by the mapping from the stimulus  $s$  to the generating function  $z$ , shown in Figure 2, and assume that both the mean of the stimulus and the offset  $\theta$  are zero. Based on observations of  $s$  and  $z$ , the linear least-squares (or reverse-correlation) RF estimate  $\hat{g}_1$  that minimizes the mean-squared error between the predicted generating function  $\hat{z}$  and the actual generating function  $z$  is given by  $\hat{g}_1 = \Phi_{ss}^{-1} \phi_{sz}$  where  $\Phi_{ss}$

is the Toeplitz matrix of the stimulus auto-covariance at different time delays, and  $\phi_{sz}$  is the cross-covariance between the stimulus and generating function (Marmarelis & Marmarelis 1978). In the absence of noise, the estimate  $\hat{g}_1$  will equal the actual RF  $g$ , and in the presence of noise,  $\hat{g}_1$  will converge to  $g$  as more data are observed.

However, when the observed response is not the generating function  $z$ , but, for example, the rectified firing rate  $\lambda$ , there is a mismatch between the model assumed in linear least-squares estimation and the actual system. Consider the mapping from  $s$  to  $\lambda$  consisting of the cascade of the linear RF  $g$  and the static nonlinearity  $f$ . Because the generating function  $z$  undergoes additional processing in the static nonlinearity, the linear least-squares RF estimate from observations of  $s$  and  $\lambda$ , which is  $\hat{g}_2 = \Phi_{ss}^{-1} \phi_{s\lambda}$ , does not necessarily equal  $\hat{g}_1$ , the RF estimate from observations of  $s$  and  $z$ . In fact, according to the result of a theorem attributed to Bussgang (1952),  $\hat{g}_2$  is a scaled version of  $\hat{g}_1$ . Bussgang's theorem states that the cross-covariance between the input to a static nonlinearity and the output of a static nonlinearity, in this case  $\phi_{z\lambda}$ , is proportional to the auto-covariance of the input to the static nonlinearity, in this case  $\phi_{zz}$ . Thus, the linear least-squares estimate of the mapping from  $z$  to  $\lambda$  is a constant  $C = \phi_{z\lambda} / \phi_{zz}$  and the best linear estimate of the two element cascade mapping  $s$  to  $\lambda$  is  $\hat{g}_2 = C \Phi_{ss}^{-1} \phi_{sz} = C \hat{g}_1$ .

As described by Stanley (2002), the scaling constant  $C$  relating  $\hat{g}_2$  to  $\hat{g}_1$  is a function of the fraction of the distribution of  $z$  that passes through the rectification. When the distribution of  $z$  is symmetric, and the mean of the stimulus and offset are zero, then this fraction is 1/2. However, if the mean of the stimulus and/or offset are non-zero, then the fraction of the generating function  $z$  that passes through the rectification is a function of the ratio of the mean of  $z$  to its standard deviation. As the mean of  $z$  increases, the scaling constant  $C$  approaches 1 as more of the signal passes through the rectification, and as the mean of  $z$  decreases, the scaling constant  $C$  approaches zero as less of the signal passes through rectification. Thus, if linear least-squares is used to estimate the RF of a neuron from extracellular observations of its response, changes in baseline membrane potential (which will affect the fraction of stimulus-driven modulations in membrane potential that trigger spikes), will be mistaken for changes in gain. Similarly, a change in the mean or contrast of the stimulus will also affect the fraction of the stimulus-driven modulations in membrane potential that trigger spikes, and can be reflected as changes in the gain of the estimated RF. This result has important implications for the analysis of adaptive encoding, as the stimulus is nonstationary, and changes in both the gain of the RF and the baseline membrane potential of the neuron have been reported in experimental observations.

The confounding effects described above can be avoided by including both the offset and the static nonlinearity in the estimation process. At a given time step  $n$ , if the stimulus and RF parameters are organized appropriately, then the discrete time spatiotemporal summation implemented by the first stage of the LN cascade model shown in Figure 2 can be written as a dot product  $y[n] = s_n^T g_n$ . The generating function  $z[n] = s_n^T g_n + \theta[n]$  can be written as the dot product  $z[n] = s_n^T g_n = [s_n \ 1]^T [g_n \ \theta[n]]$ . Because the parameter vector  $g_n$  is a linear function of the augmented stimulus vector  $s_n$ , the RF and offset can be estimated simultaneously using a variant of least-squares estimation.

To estimate the RF and offset parameters, we used an extended recursive least squares (ERLS) approach, which is based on the Kalman filter approach to state estimation (Kalman 1960; Haykin 2002). The recursive nature of ERLS allows accurate tracking of changes in the parameters of the encoding model during a single stimulus/response trial. As in any least-squares approach, ERLS seeks the parameter estimate  $\hat{g}$  that minimize the mean squared error (MSE) between the predicted response of the encoding model and the observed response of the neuron at each time step. For the encoding model in Figure 2, this amounts to

minimizing the square of  $e[n] \triangleq \lambda[n] - f(s_n^T \hat{g}_{n|n-1})$ , where the subscript  $n | n - 1$  denotes an estimate at time  $n$  given the stimulus and response history up to and including time  $n - 1$ . Because both the offset  $\theta$  and static nonlinearity  $f(\cdot)$  are included in the estimation process, the confounding effects described above are avoided. For a full description of the ERLS algorithm, see the Appendix.

It is important to note that the result of neglecting the offset and/or static nonlinearity during the estimation process is not simply a displacement of equivalent function from one component of the model to another, but a misrepresentation of the fundamental encoding properties of the neuron. For example, while the scaled version of the RF that results from estimating the RF from observations of the firing rate response without simultaneous estimation of the offset does minimize the MSE between the actual response and the predicted response for a model that does not contain an offset, the result is not functionally equivalent to a model containing the actual RF and offset. This is explicitly demonstrated in the Appendix, where the prediction error is shown to be significantly reduced for the full model.

#### *Decoupling functional mechanisms of adaptive encoding*

*Simulated responses of retinal ganglion cells to stationary white-noise.* As described above, the interactions between a neuron's spatiotemporal integration properties, baseline membrane potential, and spike threshold can have significant effects on the characterization of its response properties. To examine these effects, we used ERLS to estimate RF and offset parameters from the responses of a simulated retinal ganglion cell to white-noise stimuli under steady-state conditions, with and without consideration of the offset and/or static nonlinearity during the estimation process. Neglecting different components of the encoding model during the parameter estimation process can provide some insight into the functional significance of the interactions described above. With ERLS, the offset is neglected by estimating only the parameters of the RF (the augmented stimulus and parameter vectors  $s_n$  and  $\hat{g}_n$  are reduced to  $s_n$  and  $\hat{g}_n$ ) and the rectification is neglected by removing the static nonlinearity from the predicted response of the neuron (in this case, it reduces to  $s_n^T \hat{g}_{n|n-1}$ ).

The response of a retinal ganglion cell to a single trial of spatially uniform, zero mean, stationary white-noise was simulated using the cascade encoding model with a biphasic temporal RF with an integration window of 300 ms. The simulated responses were used to estimate the parameters of the RF, with and without simultaneous estimation of the offset and/or consideration of the static nonlinearity. The simulations allow the direct observation of the generating function (reflecting the neuron's membrane potential), which is hidden during extracellular experimental recordings.

During the estimation process, the distribution of the generating function  $z$  is inferred based on observations of the firing rate response and the structure of the underlying encoding model, and the gain of the RF estimate is based on the spread of this inferred distribution. For a given stimulus, a narrow distribution of  $z$  corresponds to an RF with a small gain, while a wide distribution of  $z$  corresponds to an RF with a large gain. Comparing the distributions of the actual and predicted generating functions under various conditions can provide some insight into the effects of the interactions between the various components of the encoding model on the parameter estimation process.

The left plot in Figure 3A shows the distributions of the actual generating function  $z$  with  $\theta/\sigma_z = -0.5$  (gray) and the predicted generating function  $\hat{z}$  (black) when both the offset and the static nonlinearity are neglected during the estimation process.

The fraction of the actual generating function that is present in the observed spike response, after offset and rectification, is shaded. Because the offset is neglected during the estimation



process, the mean of the predicted generating function  $\mu_{\hat{z}}$  is constrained to be zero (for a zero mean stimulus). Thus, the distribution of  $\hat{z}$  is centered around zero, while the distribution of  $z$  is centered around the negative offset. In addition, the standard deviation of  $\hat{z}$  is much smaller than that of  $z$  (see inset). Because the static nonlinearity is also neglected during the estimation process, the assumed encoding model that underlies the parameter estimation process specifies that the observed firing rate response is actually the generating function  $z$ . Accordingly, the RF estimate yields a predicted generating function  $\hat{z}$  with a standard deviation that matches that of the observed firing rate response and underestimates the spread of the actual generating function  $z$ .

The right plot in Figure 3A shows the RF estimates for a variety of actual offset values typical of those observed under experimental conditions (ratio of offset to standard deviation of generating function,  $\theta/\sigma_z$ , between  $-0.5$  and  $0.5$ ) when both the offset and static nonlinearity are neglected during the estimation process. The effects described above are visible in the scaling of the RF estimates (black, thickness corresponds to offset value, see legend) relative to the actual RF (gray). For zero actual offset, the gain of the RF estimate is half of that of the actual RF. As the offset increases, and more of the generating function passes through rectification, the gain of the RF estimate increases toward that of the actual RF, while as the offset decreases, and less of the generating function passes through rectification, the gain of the RF estimate decreases toward zero.

The effects of the interaction between the offset and the static nonlinearity on the estimation of the RF and offset are apparent in Figures 3B and C. When the offset is estimated simultaneously with the RF, but the static nonlinearity is neglected, as shown in Figure 3B, the assumed model again specifies that the observed firing rate response is actually the generating function  $z$ , and thus the offset  $\theta$  is estimated to be the mean of the observed response. As a result, the RF estimate is again a scaled version of the actual RF and the offset estimate is always greater than the actual offset (and approaches the correct value as the actual offset increases and more of the generating function passes through rectification).

When the static nonlinearity is included in the estimation process, but the offset is neglected, as shown in Figure 3C, the mean of the predicted generating function  $\hat{z}$  is again constrained to be zero. Now the static nonlinearity is included in the assumed encoding model and is reflected in the RF estimate. However, because the offset is neglected during the estimation process and the distribution of  $\hat{z}$  is centered around zero, the RF estimate is scaled as if exactly half of the actual generating function were rectified. When the actual offset is less than zero, as in this example, this results in an RF estimate with a gain that is smaller than that of the actual RF (as evidenced by the standard deviations of the actual and predicted generating functions shown in the inset), while, when the actual offset is greater than zero, this results in an RF estimate with a gain that is larger than that of the actual RF. In fact, the gain of the RF estimated while including the static nonlinearity and neglecting the offset during the estimation process (Figure 3C) is precisely twice that of the RF estimated when the static nonlinearity is neglected (Figures 3A and B).

When the RF and/or offset parameters are estimated under the conditions described in Figures 3A–C, the resulting model is a poor characterization of the stimulus/response transformation. However, when both the offset and the static nonlinearity are included in the estimation process, as shown in Figure 3D, the distributions of the predicted and actual generating function match, and the RF and offset estimates are accurate across the entire range of offset values. Thus, the effects of the interaction between baseline membrane potential and spike threshold on the estimation of spatiotemporal integration properties can be accounted for if the RF and offset are estimated simultaneously and the static nonlinearity is included in the estimation process. Furthermore, the inclusion of the offset dramatically improves the

ability of the model to predict the neural response to novel stimuli, as demonstrated in the Appendix.

*Simulated responses of retinal ganglion cells to white-noise with varying contrast.* The effects of the interactions described above can have a significant impact on the characterization of adaptive encoding during nonstationary stimulation, potentially masking, confounding, or creating the illusion of adaptive function. In this simulation, the response of a retinal ganglion cell (RGC) to spatially uniform white-noise was simulated as above. However, in this simulation, the contrast of the stimulus was increased midway through the 60 second trial. Such changes in stimulus contrast are followed by fast changes in gain and temporal dynamics in RGCs (over the time course of approximately 100 ms), as well as changes in baseline membrane potential with opposing fast and slow (over the time course of approximately 10 seconds) dynamics (Baccus & Meister 2002). To model these changes, simulations were conducted in which the RGC responded to the contrast switch with corresponding changes in gain (defined as the peak amplitude of the RF) and/or offset, and ERLS was used to track the changes during a single stimulus/response trial. In the following simulations and experimental studies, the static nonlinearity is included in the estimation process, and the investigation will focus on the effects of failing to simultaneously estimate both the RF and the offset. As described above, if the RF and offset are not estimated simultaneously, then changes in the baseline membrane potential or in the statistics of the stimulus can be reflected as changes in the gain of the RF estimate.

In the first simulation, both gain and offset remained fixed while the stimulus was increased from low to high contrast. The results of estimating the RF of the simulated neuron with and without simultaneous estimation of the offset are shown in Figure 4A.

While the gain of the RF estimated with simultaneous estimation of the offset (solid black) is similar to the actual gain (dashed black) and remains relatively constant throughout the trial, the gain of the RF estimated without simultaneous estimation of the offset (gray) decreases after the contrast switch. The increase in the standard deviation of the stimulus results in a decrease in ratio  $\theta/\sigma_z$  from 0.5 to 0.25, which changes the scaling of the RF estimate when the offset is not estimated simultaneously. Although the encoding properties of the neuron are completely stationary, the RF estimated without simultaneous estimation of the offset appears to adapt due to the interaction between the offset and the static nonlinearity. Note also the increased variability in the RF estimated without simultaneous estimation of the offset.

In the second simulation, the gain remained fixed after the switch from low to high contrast, while the offset  $\theta$  was increased from 0 to 10 following the switch, causing the ratio  $\theta/\sigma_z$  to increase from 0 to 0.25. The results of estimating the RF of the simulated neuron with and without the offset are shown in Figure 4B. While the gain of the RF estimated with the offset (solid black) is relatively constant and similar to the actual gain (dashed black) throughout the trial, the gain of the RF estimated without the offset (gray) increases after the contrast switch. Because the response of the neuron has been rectified and the offset is neglected during the estimation process, changes in the offset are mistaken for changes in gain. In fact, in this case, this effect is mitigated somewhat by the effects of the change in the standard deviation of the stimulus contrast described above.

In the third simulation, the fast increase in offset following the switch from low to high contrast was accompanied by a fast decrease in gain, causing the ratio  $\theta/\sigma_z$  to increase from 0 to 0.5. The results of estimating the RF of the simulated neuron with and without the offset are shown in Figure 4C. While the gain of the RF estimated with the offset (solid black) tracks the decrease in the actual gain (dashed black), the gain of the RF

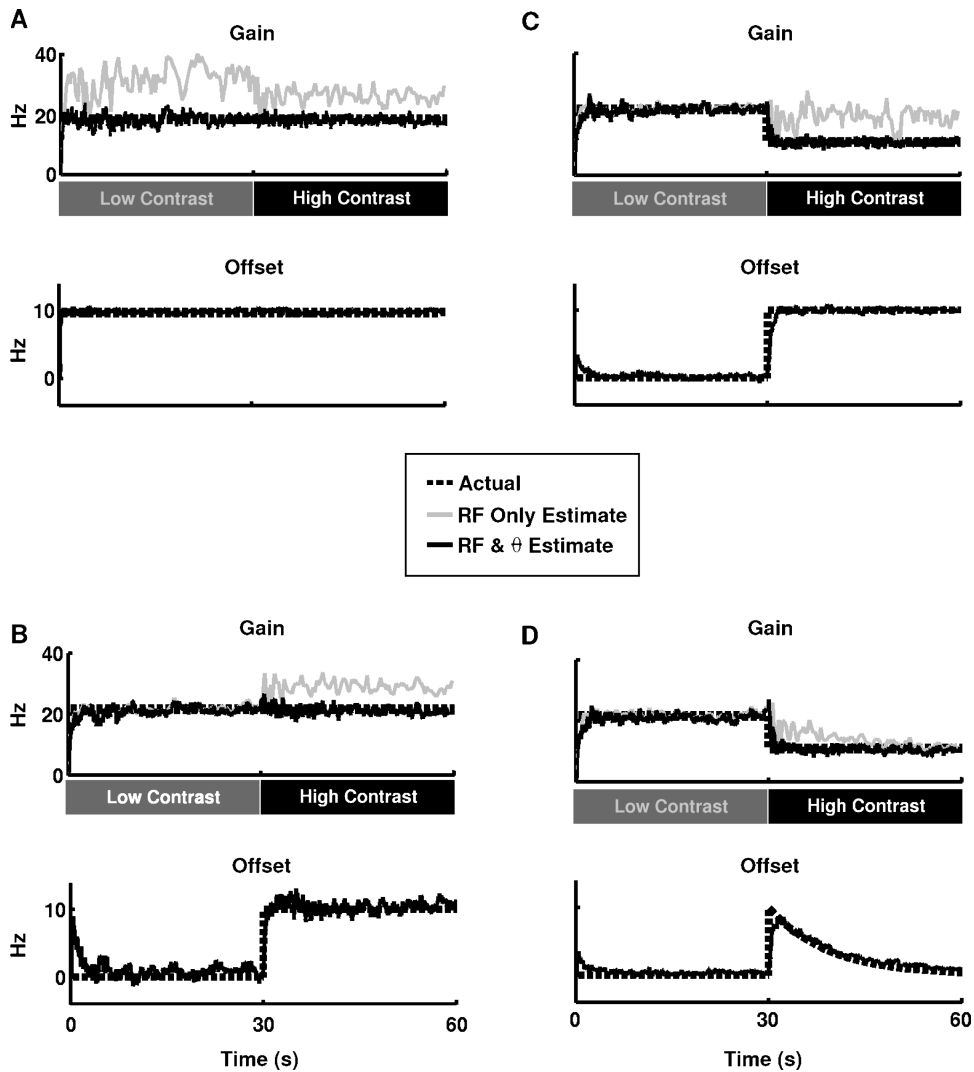


Figure 4. RF and offset estimates from simulated responses to contrast-switching white-noise. The response of a retinal ganglion cell to spatially uniform, contrast switching white-noise was simulated and the responses were used to estimate the RF and offset of the simulated neuron. The contrast switch in the stimulus was accompanied by corresponding changes in the gain and offset of the simulated neuron. (A) RF and offset estimates for a simulated neuron with gain and offset held fixed throughout the trial. The RF estimates with (black) and without (gray) simultaneous estimation of the offset are shown in the top plot, along with the offset estimate in the bottom plot. In both plots, the actual value of the quantity to be estimated is also shown (dashed black). The contrast of the stimulus is indicated under the time axis of the top plot. Similar plots are shown for simulations in which the simulated neuron responded to the contrast switch with (B) a fast change in offset, (C) fast changes in gain and offset, and (D) a fast change in gain and fast and slow changes in offset.

estimated without the offset remains relatively constant following the contrast switch. In this case, the actual decrease in gain is countered by the apparent increase in gain that results from neglecting the offset during the estimation process. Thus, the interactions between the RF, offset, and static nonlinearity cause the adaptive changes to be completely masked.

Finally, in the fourth simulation, a slow decrease in offset is added to the fast changes in gain and offset in the previous simulation. In this example, the offset decreases exponentially toward its original value of zero in the 30 seconds following the change in contrast and corresponding fast increases in gain and offset, reflecting the adaptive behavior observed in actual retinal ganglion cells. The ratio  $\theta/\sigma_z$  increases from 0 to 0.5 directly following the increase in contrast, and gradually decays to zero. The results of estimating the RF of the simulated neuron with and without the offset are shown in Figure 4D. While the gain of the RF estimated with the offset (solid black) tracks the fast decrease in the actual gain (dashed black), the gain of the RF estimated without the offset decreases slowly after the contrast switch. In this case, the interactions between the RF, offset, and static nonlinearity result in the fast adaptive changes being completely masked and the slow change in offset being reflected as a slow change in gain.

*Experimental responses of retinal ganglion cells to white-noise with varying contrast.* Similar effects of the interactions described above can be demonstrated under experimental conditions, using the response of RGCs to a contrast switching stimulus. Spatially uniform Gaussian white-noise was projected onto an isolated salamander retina and ganglion cell action potentials were recorded extracellularly. These experiments were performed in the laboratory of Markus Meister at Harvard University and details of the preparation are given in (Baccus & Meister 2002). A new luminance value for the stimulus was chosen every 30 ms and the contrast was switched from 5% to 35% every 30 seconds.

Figure 5A shows 3 minutes of the white-noise stimulus used in the experiment.

The estimates of gain and offset track the changes following stimulus transitions during a single trial, as shown in Figures 5B and C. The average of these estimates over 24 repeats of the same feature transitions are shown in Figure 5D and E (black). For comparison, the gain of the RF estimated without simultaneous estimation of the offset is shown in gray. As expected, the simultaneous estimates of RF and offset capture the fast changes in gain, as well as opposing fast and slow changes in offset. Neglecting the offset during the estimation process causes the fast changes in gain to be partially masked by the fast changes in offset (the fast gain changes in the ‘RF Only’ estimate are smaller than those in the ‘RF &  $\theta$ ’ estimate), and the slow changes in offset to be reflected as slow changes in gain.

## Discussion

The results presented above demonstrate the profound effects of the interactions between spatiotemporal integration properties, baseline membrane potential and spike threshold on the response properties of adaptive neurons. Using an encoding model with an adaptive spatiotemporal RF and offset, we have demonstrated that the function of multiple adaptive mechanisms can be uniquely identified during a single trial of nonstationary stimulus/response data. We have also shown that misspecification of the encoding model underlying the parameter estimation process (estimating the RF without considering the offset and/or static nonlinearity) can obscure adaptive function. Because of the rectification properties of visual neurons, changes in baseline membrane potential and/or the statistics of the stimulus can be reflected as changes in gain if the offset and static non-linearity are not included in the estimation process. These results are consistent with those of other studies that have investigated the effects of spiking dynamics on the characterization of linear response properties. For example, studies have shown that both refractoriness (Berry & Meister 1998) and changes in membrane conductance (Pillow & Simoncelli 2003) can affect the estimation of RFs.

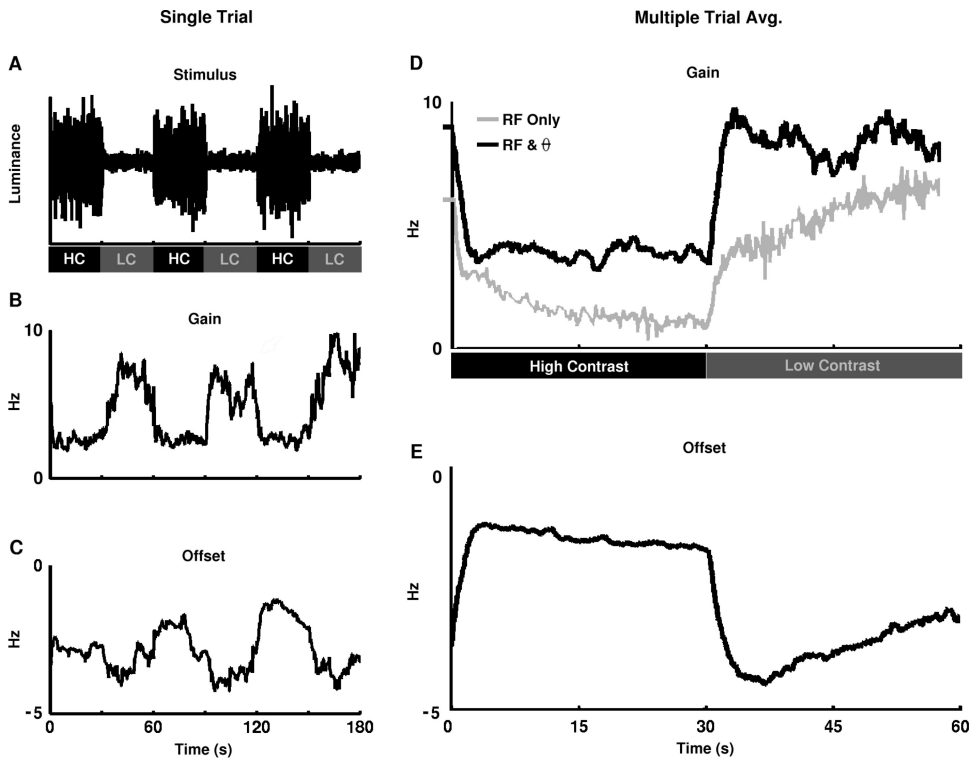


Figure 5. RF and offset estimates from experimental responses to contrast-switching white-noise. Experimentally observed responses of a salamander retinal ganglion cell to a contrast switching stimulus were used for adaptive estimation of encoding properties. (A) 3 minutes of the spatially uniform Gaussian white-noise stimulus. A new luminance value for the stimulus was chosen every 30 ms and the contrast was switched between 5% and 35% every 30 seconds. (B) The gain of the RF estimate (with simultaneous estimation of offset) during the 3 minute interval. (C) The offset estimate during the same 3 minute interval. (D) The average gain of the RF estimate over 24 repeats of the same contrast transitions (12 minutes) with (black) and without (gray) simultaneous estimation of the offset. (E) The average of the offset estimate over the same 12 minute interval.

These results have significant implications for the study of adaptive function. There are a number of recent studies that have reported adaptive phenomena similar to those described here (Carandini & Ferster 1997; Sanchez-Vives et al. 2000; Chander & Chichilnisky 2001; Kim & Rieke 2001; Zaghoul et al. 2005), and it appears that adaptation may be a ubiquitous property of sensory encoding. We have distinguished between two types of adaptation (changes in spatiotemporal integration properties and changes in baseline membrane potential) based on their functional properties. However, the origins of the two forms of adaptation, the neural mechanisms that control them (local modulation of synaptic input strength, large-scale changes in network properties, etc.), and their functional roles are still the subject of controversy (Baccus & Meister 2004; Demb 2002). For example, studies of contrast adaptation in the retina have produced conflicting results regarding the persistence of the decrease in gain that follows an increase in contrast. While some studies suggest that, if the contrast remains high, then the decrease in gain will persist (Victor 1987; Baccus & Meister 2002), others suggest that the gain will continue to decline (Smirnakis et al. 1997; Brown & Masland 2001). As shown in a recent study by (Baccus & Meister 2002) using intracellular recordings, the gain change that follows a contrast switch does indeed persist, and is accompanied by corresponding fast and slow changes in baseline membrane potential. As

our results have shown (see Figure 5), in estimating the RF from the experimental responses of retinal ganglion cells to a change in stimulus contrast without simultaneous estimation of the offset, slow adaptive changes in baseline membrane potential can appear as slow changes in gain. Thus, the apparent continued decline in gain observed in the studies described above may in fact have been a reflection of changes in baseline membrane potential, as the RFs in those studies were estimated without simultaneous estimation of the offset.

The framework we have presented enables the analysis of adaptive function with encoding models and parameter estimation approaches that are consistent with experimental observations. Using this framework, the function of multiple simultaneously active adaptive mechanisms can be accurately characterized. With the addition of a single parameter to the typical LN cascade model of visual encoding, the true dynamics of the RF can be decoupled from changes in baseline membrane potential, and the confounding effects of adaptation be avoided. There are indications that adaptive encoding is a fundamental principle of sensory systems and the application of this framework at successive stages in the visual pathway, as well as in other sensory systems, may provide insight into the neural mechanisms that underly adaptive function.

## Appendix

### A1: A detailed description of the LN cascade encoding model

The firing activity of many types of sensory neurons can be characterized by a cascade of a linear receptive field (RF) and a static nonlinearity (Hunter & Korenberg 1986; Reid et al. 1997; Chichilnisky 2001; Baccus & Meister 2002). Here, a particular form of the LN cascade model, shown in Figure 2, is developed based on observations of adaptive function in the early visual pathway (Shapley & Enroth-Cugell 1984; Shapley & Victor 1978; Movshon & Lennie 1979; Carandini & Ferster 1997; Sceniak et al. 1999; Baccus & Meister 2002; Solomon et al. 2004; Zghloul et al. 2005). Each component of the LN cascade model is described in detail below.

#### *Linear spatiotemporal receptive field*

In the first stage of the LN cascade encoding model shown in Figure 2, the visual stimulus is passed through the linear spatiotemporal RF. The visual stimulus is described in terms of the spatiotemporal light intensity, sampled at time interval  $\Delta t$  and at a fixed spatial resolution. The spatiotemporal signal is denoted  $s[p, n]$ , where  $p$  represents the grid index of a pixel on the screen and  $n$  is the index of the time sample. Note that pixel refers not to the atomic display units of the monitor, but, for instance, to uniform squares in a white-noise checkerboard, subtending a fixed visual angle. No assumptions are made about the statistics of the stimulus, as natural signals are often nonstationary and correlated over space and time.

For many classes of neurons in the early visual pathway, visual inputs are summed linearly across the extent of the receptive field in space and over the recent history of the stimulus in time. The linear spatiotemporal receptive field (RF) represents this spatiotemporal summation, and is denoted in the model by the linear filter  $g_n[p, m]$ . The filter represents  $P$  (total pixels in stimulus) separate temporal filters each with  $M$  (length of temporal RF) lags. The subscript  $n$  denotes the dependence on time, allowing for modulation of RF properties by adaptation processes. If  $s_n$  and  $g_n$  are organized appropriately, then the discrete time spatiotemporal summation can be written as a dot product  $y[n] = s_n^T g_n$ , where  $s_n$  and  $g_n$  are the

column vectors:

$$s_n = [s[P, n - M + 1], s[P - 1, n - M + 1], \dots, s[1, n - M + 1], s[P, n - M + 2], \dots, s[1, n]]^T$$

$$g_n = [g_n[P, M], g_n[P - 1, M], \dots, g_n[1, M], g_n[P, M - 1], \dots, g_n[1, 1]]^T$$

where  $T$  denotes matrix transpose. The parameter values are unconstrained, so that adaptive changes in gain and spatiotemporal tuning properties can be captured.

### *Offset*

The output  $y[n]$  of the RF describes the projection of the spatiotemporal visual stimulus onto the univariate process that gives rise to the neuronal activity. Because of the rectification properties of neurons, the stimulus-driven modulations that are captured by  $y[n]$  can result in different responses depending on the baseline membrane potential. In the encoding model shown in Figure 2, variations in baseline membrane potential are reflected in the time-varying offset  $\theta[n]$ .

### *Static nonlinearity*

The filtered and offset stimulus  $z[n]$ , known as the *generating function*, is projected onto a non-negative firing rate  $\lambda[n]$  through a rectifying static nonlinearity  $f(\cdot)$ . The model used here (variable offset, fixed rectification threshold) is functionally equivalent to a rectifier with a variable threshold. However, the former more accurately reflects the underlying physiology (adaptive changes have been observed in baseline membrane potential, but not in the threshold for spike generation (Carandini & Ferster 1997; Carandini & Ferster 2000)). For many visual neurons (including those analyzed in this study), the static nonlinearity (as estimated from responses to stationary white-noise using reverse correlation and a graphical fitting method (Chichilnisky 2001)) closely matches linear, half-wave rectification. Thus, here the static nonlinearity  $f(\cdot)$  is assumed to be a linear half-wave rectifier, where

$$f(z) = \begin{cases} z, & z \geq 0 \\ 0, & z < 0 \end{cases}$$

It should be noted that, although a linear half-wave rectifier is imposed here, the ERLS approach for estimating the parameters of the encoding model is developed for a general static nonlinearity  $f(\cdot)$ , the specific form of which should be chosen based the properties of the system under investigation. Model parameters were estimated using simulated visual neurons in which the static nonlinearity had a different shape, such as a hyperbolic tangent rectifier or a sigmoid, and the results were similar to those obtained with linear rectification.

It should also be noted that the LN cascade model described here only provides accurate description of firing rate on timescales that are larger than that of the neuron's relative refractory period. On a finer timescale, changes in the statistics of the stimulus can alter the trial to trial variability of the neural response (Reich et al. 2001). However, the description of such phenomena is beyond the scope of this paper.

## **A2: A detailed description of extended recursive least-squares**

From the LN cascade model in Figure 2, the generating function (without noise)  $z[n] = s_n^T g_n + \theta[n]$  can be written as the dot product  $z[n] = s_n^T g_n = [s_n \ 1]^T [g_n \ \theta[n]]$ . The variable components of the cascade encoding model described by the  $M \times P + 1$  parameters of  $g_n$

can be adaptively estimated from stimulus/response data using an extended version of the recursive least-squares approach (ERLS). The ERLS algorithm for estimating the parameters of the model in Figure 2 is given by:

$$\begin{aligned}
 e[n] &= \lambda[n] - f(s_n^T \hat{g}_{n|n-1}) && \text{Prediction Error} \\
 G_n &= \frac{K_{n|n-1} s_n}{s_n^T K_{n|n-1} s_n + 1} && \text{Update Gain} \\
 \hat{g}_{n+1|n} &= \hat{g}_{n|n-1} + G_n e[n] && \text{Update Parameter Estimates} \\
 K_{n+1|n} &= K_{n|n-1} - G_n s_n^T K_{n|n-1} + \sigma_q^2 [N] I && \text{Update Inverse of Stimulus} \\
 &&& \text{Autocovariance}
 \end{aligned}$$

At each time step, the gain  $G$  is calculated based on the estimate of the inverse of the stimulus autocovariance matrix  $K$  (permitting the use of correlated stimuli) and combined with the prediction error  $e$  to update the parameter estimate  $\hat{g}$ . To initialize the algorithm, the initial conditions  $\hat{g}_{0|-1} = 0$  and  $K_{0|-1} = \delta \times I$  are used, where  $I$  is the appropriately dimensioned identity matrix. The regularization parameter  $\delta$  affects the convergence properties and steady-state error of the ERLS estimate. By placing a lower bound on the condition number of the stimulus autocovariance matrix, the regularization parameter  $\delta$  places a smoothness constraint on the parameter estimate, removing some of the error introduced by highly correlated natural stimuli. For parameter estimates computed here,  $\delta$  was set to  $10^{-4}$ . A discussion of choosing the value of  $\delta$  based on the signal-to-noise ratio of the system under investigation is given in (Haykin 2002).

The prediction error  $e$  is the difference between the observed and predicted firing rates. Given the stimulus and the current estimate of the RF, the expected firing rate is:

$$\begin{aligned}
 E\{\lambda[n]|s_n, \hat{g}_{n|n-1}\} &= \int_{\lambda} \lambda[n] p(\lambda[n]|s_n, \hat{g}_{n|n-1}) d\lambda[n] \\
 &= \int_v f(s_n^T \hat{g}_{n|n-1} + v[n]) p(v[n]) dv[n]
 \end{aligned}$$

where  $p(\lambda[n]|s_n, \hat{g}_{n|n-1})$  is the probability density function of the predicted response conditioned on the current stimulus and estimated model parameters. Through a series expansion about  $s_n^T \hat{g}_{n|n-1}$ , the expectation can be approximated as  $E\{\lambda[n]|s_n, \hat{g}_{n|n-1}\} \approx f(s_n^T \hat{g}_{n|n-1})$ . This approximation is valid when the signal to noise ratio in the system is large (the stimulus-driven modulations in membrane potential are much larger than the intrinsic noise), as is typically the case in visual neurons under dynamic stimulation. In the event that this approximation is not valid, the integral expression for the expected firing rate can be evaluated at each time step.

The learning rate  $\sigma_q^2[n]$  should reflect the expected change in the parameter values over a given interval. For all parameter estimates computed here, it was assumed that the parameters change independently of one another and at equal rates. For parameter estimation under steady-state condition,  $\sigma_q^2[n]$  was set to the constant value 0.001. For parameter estimation under adaptive condition,  $\sigma_q^2[n]$  was increased to a value of 0.01 for the 300 ms following a contrast switch, to capture fast adaptive changes. For range of RFs shown here, these values for  $\sigma_q^2[n]$  correspond to between 0.002% and 1% of the gain (peak amplitude). For further discussion of the effects of the choice of the adaptive learning rate  $\sigma_q^2[n]$  on adaptive parameter estimation, see (Lesica & Stanley 2005).

### A3: Encoding models estimated with and without offset are not functionally equivalent

The results presented here have demonstrated that, when the underlying system has a non-zero offset and rectifying static nonlinearity, estimating the RF without simultaneous estimation of the offset produces a scaled version of the actual RF. The purpose of this section is to demonstrate that, although the scaled version of the RF minimizes the MSE between the predicted and actual responses for an assumed model structure with no offset, an encoding model containing the scaled RF and no offset is not functionally equivalent to one containing the actual RF and offset. This is illustrated by the results of the simulations shown in Figure 6.

The response of a retinal ganglion cell to a 60 second segment of spatially uniform, stationary white-noise was simulated with offset values of  $-10$  Hz and  $10$  Hz. The responses were used for RF estimation with ERLS, with and without simultaneous estimation of the offset. The RFs estimated without simultaneous estimation of the offset were used in the encoding

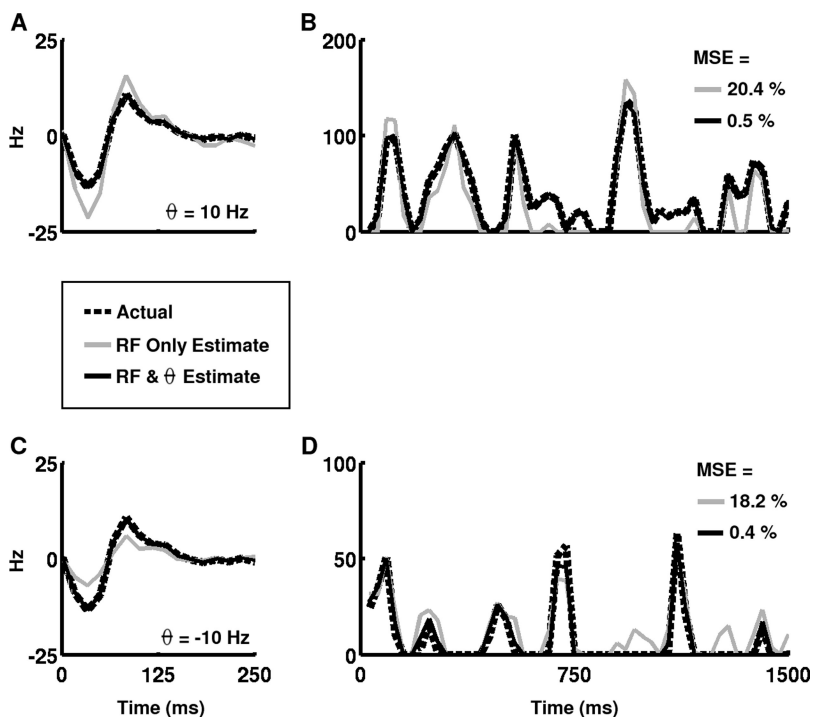


Figure 6. Encoding models including RFs estimated with and without simultaneous estimation of the offset are not functionally equivalent. The response of a retinal ganglion cell to spatially uniform, stationary white-noise was simulated with offset values of  $-10$  Hz and  $10$  Hz. The responses were used to estimate the RF of the simulated neuron with and without simultaneous estimation of the offset, and the results were used in the cascade encoding model to predict the response of the neuron. (A) The RF estimates with (solid black) and without (gray) simultaneous estimation of the offset are shown, along with the actual RF (dashed black), for the simulation with an offset value of  $10$  Hz. (B) Actual and predicted responses of the simulated neuron over a  $1.5$  second interval. The response from the encoding model with the accurate RF and offset is shown in solid black. The response from the model with the scaled RF and no offset is shown in gray. The actual response is shown in dashed black. The MSE between the predicted and actual responses over the entire  $60$  second trial are also shown. Similar results for a simulated neuron with an offset value of  $-10$  Hz are shown in (C) and (D).

model with an offset of zero, and the RFs estimated with simultaneous estimation of the offset were used in the encoding model with the corresponding estimated offset value. For all estimates in this example, the static nonlinearity was included in the estimation process.

Figure 6A shows the RF estimates for the simulation with an offset of 10 Hz. As expected, the RF estimated with simultaneous estimation of the offset (solid black) matches the actual RF (dashed black), while the RF estimated without simultaneous estimation of the offset (gray) is a scaled version of the actual RF. As illustrated in Figure 3, estimating the RF without simultaneous estimation of the offset when the static nonlinearity is included in the estimation process and the actual offset is positive results in an RF estimate with a larger gain than the actual RF. The results of using the two RF estimates in the cascade encoding model to predict the response of the neuron are shown in Figure 6B. The figure shows the actual firing rate of the neuron  $\lambda$  (dashed black) and the predicted firing rate  $\hat{\lambda}$  generated by the models containing the RFs estimated with (solid black) and without (gray) simultaneous estimation of the offset. While the prediction from the encoding model with the RF estimated with simultaneous estimation of the offset closely matches the actual response (MSE = 0.5% of response variance), the prediction from the model with the RF estimated without simultaneous estimation of the offset contains substantial error (MSE = 20.4%). Similar results are shown for the simulated neuron with an offset value of  $-10$  Hz in Figures 6C and D. In this case, the RF estimated without simultaneous estimation of the offset has a smaller gain than the actual RF, as the actual offset is negative. Again, the prediction from the encoding model with the RF estimated with simultaneous estimation of the offset closely matches the actual response (MSE = 0.4% of response variance), while the prediction from the model with the RF estimated without simultaneous estimation of the offset contains substantial error (MSE = 18.2%). Thus, although the scaled RF estimated without simultaneous estimation of the offset does minimize the prediction error for the encoding model with zero offset, the result is not an accurate description of the underlying system.

## Acknowledgments

The authors would like to thank Steve Baccus and Markus Meister for the use of the salamander retinal data. The authors would also like to thank the members of the laboratory of Markus Meister, Uri Eden and Daniel Butts for helpful conversations during various stages of this work. This work was supported by National Geospatial-Intelligence Agency Grant HM1582-05-C-0009.

## References

- Baccus SA, Meister M. 2002. Fast and slow contrast adaptation in retinal circuitry. *Neuron* 36:909–919.
- Baccus SA, Meister M. 2004. Retina versus cortex: contrast adaptation in parallel visual pathways. *Neuron* 42:5–7.
- Berry MJ, Meister M. 1998. Refractoriness and neural precision. *J Neurosci* 18:2200–2211.
- Brenner N, Bialek W, de Ruyter van Steveninck R. 2000. Adaptive rescaling maximizes information transmission. *Neuron* 26:695–702.
- Brown SP, Masland RH. 2001. Spatial scale and cellular substrate of contrast adaptation by retinal ganglion cells. *Nat Neurosci* 4:44–51.
- Busgang JJ. 1952. Crosscorrelation functions of amplitude distorted gaussian signals. MIT Res Lab Elec Tech Rep 216:1–14.
- Carandini M, Ferster D. 1997. A tonic hyperpolarization underlying contrast adaptation in cat visual cortex. *Science* 276:949–952.
- Carandini M, Ferster D. 2000. Membrane potential and firing rate in cat visual cortex. *J Neurosci* 20:470–484.

- Chander D, Chichilnisky EJ. 2001. Adaptation to temporal contrast in primate and salamander retina. *J. Neurosci.* 21:9904–9916.
- Chichilnisky EJ. 2001. A simple white noise analysis of neuronal light responses. *Network* 12:199–213.
- Demb JB. 2002. Multiple mechanisms for contrast adaptation in the retina. *Neuron* 36:781–783.
- Fairhall AL, Lewen GD, Bialek W, de Ruyter van Stevenick RR. 2001. Efficiency and ambiguity in an adaptive neural code. *Nature* 412:787–790.
- Haykin S. 2002. *Adaptive Filter Theory*. New Jersey, Prentice Hall.
- Hunter I, Korenberg M. 1986. The identification of nonlinear biological systems: Wiener and hammerstein cascade models. *Biol Cybern* 55:135–144.
- Kalman RE. 1960. A new approach to linear filtering and prediction problems. *Transactions of the ASME—J Basic Engineering* 82:35–45.
- Kim KJ, Rieke F. 2001. Temporal contrast adaptation in the input and output signals of the salamander retinal ganglion cells. *J Neurosci* 21:287–299.
- Lesica NA, Stanley GB. 2005. Tracking receptive field modulation during natural stimulation. *IEEE Trans Neural Syst Rehab Eng* 13:194–200.
- Marmarelis PZ, Marmarelis VZ. 1978. *Analysis of Physiological Systems*. New York: Plenum.
- Movshon JA, Lennie P. 1979. Pattern-selective adaptation in visual cortical neurones. *Nature* 278:850–853.
- Pillow JW, Simoncelli EP. 2003. Biases in white noise analysis due to non-poisson spike generation. *Neurocomputing* 52–54:109–115.
- Reich DS, Mechler F, Victor JD. 2001. Formal and attribute-specific information in primary visual cortex. *J Neurophysiol* 85:305–318.
- Reid RC, Victor JD, Shapley RM. 1997. The use of m-sequences in the analysis of visual neurons: linear receptive field properties. *Vis Neurosci* 14:1015–1027.
- Sanchez-Vives MV, Nowak LG, McCormick DA. 2000. Membrane mechanisms underlying contrast adaptation in cat area 17 in vivo. *J Neuroscience* 20:4267–4285.
- Sceniak MP, Ringach DL, Hawken MJ, Shapley R. 1999. Contrast's effect on spatial summation by macaque v1 neurons. *Nature Neurosci* 2:733–739.
- Shapley R., Enroth-Cugell C. 1984. Visual adaptation and retinal gain controls. *Prog Ret Res* 3:263–346.
- Shapley RM, Victor JD. 1978. The effect of contrast on the transfer properties of cat retinal ganglion cells. *J Physiol* 285:275–298.
- Smirnakis SM, Berry MJ, Warland DK, Bialek W, Meister, M. 1997. Adaptation of retinal processing to image contrast and spatial scale. *Nature* 386:69–73.
- Solomon SG, Pierce JW, Dhruv NT, Lennie P. 2004. Profound contrast adaptation early in the visual pathway. *Neuron* 42:155–162.
- Stanley GB. 2002. Adaptive spatiotemporal receptive field estimation in the visual pathway. *Neural Computation* 14:2925–2946.
- Victor JD. 1987. The dynamics of the cat retinal  $\times$  cell centre. *J Physiol* 386:219–246.
- Zaghloul KA, Boahen K, Demb JB. 2005. Contrast adaptation in subthreshold and spiking responses of mammalian  $\gamma$ -type retinal ganglion cells. *J Neurosci* 24:860–868.